Velocity dependence of the cross sections for Penning and associative ionization of H and D atoms by He(2^3S) metastable atoms

J. Fort,* J. J. Laucagne, A. Pesnelle, and G. Watel
Service de Physique Atomique, Centre d'Etudes Nucléaires de Saclay, Boite Postale 2, 91190 Gif sur Yvette, France
(Received 16 September 1977)

The velocity dependence of both the Penning and associative ionization cross sections σ_{PI} and σ_{AI} for the He(2^3S) + H interacting system as well as total ionization cross section σ_{TI} is measured for the relative velocity range 1900–5300 m/sec (0.015–0.10 eV energy range) in a crossed-beam experiment by a time-of-flight technique. Characteristic cross-section ratios σ_{AI}/σ_{TI} and the relative magnitudes of the cross sections σ_{AI}, σ_{PI}, and σ_{TI} are reported. The experimental results concerning the total ionization cross section are in very good agreement with previous theoretical work, but the experimental values of the ratio σ_{AI}/σ_{TI} are found to be higher than theoretical values, especially at low energies. A numerical solution of the Schrödinger equation with a complex potential is performed to interpret both the results on the He(2^3S) + H system and our previously published results on the He(2^1S) + H system. A truncated width is used for the calculation of the associative cross sections. It is observed that an exponentially shaped autoionization width $\Gamma(R) = Ae^{-R/B}$ is satisfactory and that the width for the He(2^1S) + H system is nearly equal to the width for the He(2^3S) + H system.

I. INTRODUCTION

The Penning and associative processes are described by the following reactions:

$$\mathrm{He}(2^3S) + H \xrightarrow{\sigma_{PI}} H^+ + \mathrm{He} + e$$
$$\xrightarrow{\sigma_{AI}} \mathrm{HeH}^+ + e\,.$$

The velocity dependence of the Penning and associative ionization cross sections for the He(2^1S) + H interacting system has been presented in Ref. 1. In the present work, we have obtained the velocity dependence of the Penning and associative ionization cross sections for the He(2^3S) + H interacting system in order to complete the experimental study of the simplest three-electron diatomic system involving these processes. Thus, comparison with the theoretical approaches can be extended to the triplet case for which the various potential curves, the autoionization width and the consequent ionization cross sections are available in the literature.[2-9] Until now, comparison has not been easy because most of the experiments yielded cross sections averaged over the velocity distributions of the colliding atoms at one temperature. Shaw *et al.*[10] made a measurement of the quenching of He(2^3S) in a flowing afterglow at 300 °K, and Howard *et al.*[11] measured σ_{PI} and σ_{AI} at an average kinetic energy of 0.37 eV in a crossed-beam apparatus. Only Magnuson *et al.*[12] attempted to point out the role of the relative kinetic energy of He(2^3S) and H atoms in the σ_{AI} cross section.

We have measured the velocity dependence of σ_{PI} and σ_{AI} in the 1900–5300 m/sec relative velocity range which corresponds to the 0.015–0.11 eV relative kinetic energy range, in a crossed-beam experiment by a time-of-flight technique (TOF). The results presented in this paper are a useful test of the different calculations of cross sections published to date. All these calculations are formulated inside the same model in terms of a local complex potential, but they differ either in the method (classical[2-8] or semi-classical[4-7]) or in the data used [incoming- and outgoing-channel potential curves $V^*(R)$ and $V^+(R)$, autoionization width $\Gamma(R)$].

We have developed a pure quantum calculation of the total ionization cross sections σ_{TI} for both systems He(2^3S) + H and He(2^1S) + H by solving numerically the Schrödinger equation into which has been introduced the complex potential $V^*(R) - i\frac{1}{2}\Gamma(R)$. The associative cross section σ_{AI} is obtained by the same method except that now a truncated width $\Gamma_{AI}(R)$ replaces $\Gamma(R)$ in the Schrödinger equation. The coupling width $\Gamma_{AI}(R)$ is defined via the classical criterion

$$R > R_{AI}, \quad \Gamma_{AI}(R) = 0\,,$$
$$R < R_{AI}, \quad \Gamma_{AI}(R) = \Gamma(R)\,.$$

This method neglects the "survival factor" which appears in the classical formulation.

II. EXPERIMENT

The same time-of-flight technique as used in our work on Ar (Refs. 13 and 14) and He(2^1S) + H (Ref. 1) has been employed. Some modifications have been made to the apparatus concerning the interaction chamber. Ions produced in this chamber can be extracted either directly into an electron multipli-

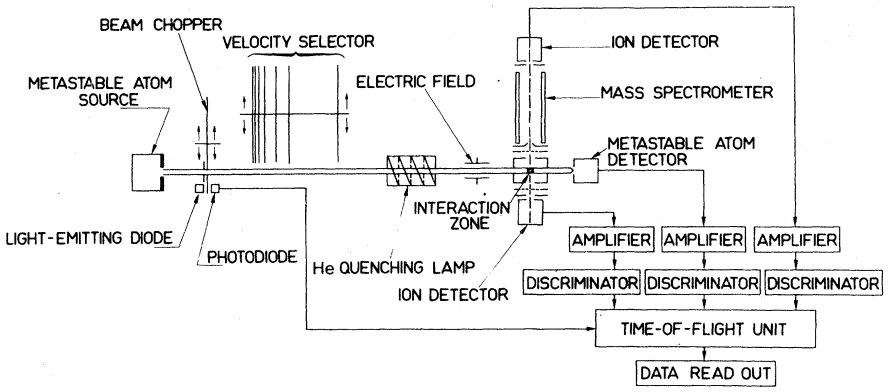

FIG. 1. Schematic diagram of the apparatus. The target H atom beam enters the interaction chamber in a plane perpendicular to the plane of the diagram. For clarity, the distances are not drawn to scale.

er for total ion-production measurement or into a quadrupole mass analyzer for Penning or associative ion-production measurement.

The metastable beam and the H target beam are produced as in our previous paper on $He(2\,^1S)+H$. The difference with the previous work is that fuller measurements have been necessary to collect the Penning ions produced by $He(2\,^3S)$, the energy of which can be as high as 2 eV, and verifications have been made by measuring the total ion production. A schematic diagram of the apparatus is shown on Fig. 1.

In the theoretical model usually employed, since the ejected electron takes up all the excess potential energy, the kinetic energy of the Penning ions is given by

$$E_C^+ = E_C + V^*(\infty) - V^*(R) + V^+(R)\,,$$

where $V^+(\infty)$ is taken as zero. E_C is the relative kinetic energy of He^*+H. $V^*(R)$ and $V^+(R)$ are the He^*+H and $He+H^+$ potential curves, respectively. Calculations of $V^*(R)$ for the triplet and singlet cases have been done by Miller *et al.*[2] and Fujii *et al.*,[3] but the curves obtained by Miller *et al.* seem more trustworthy than the others. $V^+(R)$ is the $He+H^+$ potential curve. As a result of the relative position of the wells of $V^*(R)$ and $V^+(R)$, E_C^+ can reach values of the order of magnitude of the well depth of $V^*(R)$, i.e., 1.8 eV for the triplet and 0.4 eV for the singlet [for He^*-H system, in the thermal velocity range the kinetic energy in the laboratory coordinates $E_c^+(\text{lab})$ is close to the kinetic energy in the center-of-mass coordinates E_c^+].

In our preceding paper, the interaction chamber was biased to $V_c=+20$ V (relative to ground), the focusing diaphragm to $V_f=-12$ V, and the quadrupole entrance diaphragm itself was grounded. This was to ensure the efficient collection of low-energy ions [$E_c^+(\text{lab})=0.5$ eV is the threshold for efficient collection] such as Ar^+ produced by $He(2\,^1S)$ and $He(2\,^3S)$, H^+ produced by $He(2\,^1S)$ and all the associative ions and to mass analyze them with maximum transmission through the quadrupole mass spectrometer. In a first step, we have observed that the shape of the TOF spectra of these low-energy ions is not sensitive to V_c varying from 20 to 100 V, but that the count rate at $V_c=100$ V was a factor of $2\pm10\%$ lower than at $V_c=20$ V. This signifies that the transmission of the quadrupole decreases when the energy of the ions at its entrance diaphragm, which is close to V_c, increases.

In a second step, we have observed that the TOF spectrum of H^+ ions produced by He $(2\,^3S)$ is strongly perturbed when V_c varies from 20 to 100 V (saturation is observed from 90 V), which proves that these ions actually have energies larger than 0.5 eV. Therefore, in order to obtain the correct complete TOF spectrum of these H^+ ions, the raw spectrum obtained at $V_c=+100$ V is multiplied by a factor of 2 to take into account the loss of transmission between $V_c=20$ and 100 V. In a third step, a thorough study of the total ion production is performed. The ions are extracted from the interaction chamber which is biased at $V_c=+100$ V, through a 10.2-mm-diam aperture positioned opposite the other 10.2-mm-diam aperture which leads to the quadrupole (see Fig. 1). The ions are focused by an electrostatic lens consisting of the extraction aperture, a 6-mm-diam grid biased at -50 V and a 10-mm-diam grounded diaphragm. The distance between the elements is 2 mm. Field lines thus produced inside the interaction chamber are such that most ions [$E_c^+(\text{lab}) \leq 2$ eV] are extracted, including thermal ions. The ions are detected by an electron multiplier (Spiraltron Bendix 4219 X), which replaces the electron gun of the previous experiment.[1] Electronics are similar to those employed in Ref. 1.

III. RESULTS

A. Data for $He(2\,^3S) + H$

Since the $He(2\,^1S)$ component of the metastable beam can be quenched with the helium discharge lamp, the signal corresponding to $He(2\,^3S)$ atoms is derived by making observations with the lamp continuously on. The TOF spectra of the H^+ and HeH^+ ions are shown in Fig. 2. The TOF spectrum of the $He(2\,^3S)$ atoms is similar to $He(2\,^1S)$ one published previously,[1] as we noted in our work on Ar.[14]

Photons are emitted by the metastable atom source. They produce H^+ ions in the interaction zone by photoionization. Accumulation of data with no delay gives a H^+ photoion peak in the H^+ TOF spectrum and a photon peak in the He* TOF spectrum, both having the gate-function shape. The photoion peak is delayed by the ion transit time in the mass analyzer. The zero of the time scales is given by the middle of the photon or photoion peak.

Furthermore, we have verified that the extraction and the mass selection of the ions did not modify their TOF spectra by using the TOF technique and a velocity selector for the metastable beam (which has not been used elsewhere in the present work). A triangular He* TOF spectrum is thus obtained, whose base width is related to the resolution of the velocity selector ($R \simeq 10\%$). We have observed a similar triangular H^+ TOF spectrum.

Although it has been observed that the H^+ ion production by $He(2\,^3S) + H_2$ collisions is negligible compared to the number of H^+ ions produced by $He(2\,^3S) + H$ collisions (a factor of 10^{-3}), the contribution of the H_2 molecules remaining in the target beam to HeH^+ ion production is not negligible (a factor of 10^{-1}). In order to obtain the HeH^+ TOF spectrum resulting from only $He(2\,^3S) + H$ collisions, we have subtracted from the HeH^+ TOF spectrum resulting from $He^* + H, H_2$ collisions (hydrogen rf discharge on) the HeH^+ TOF spectrum resulting from $He^* + H_2$ collisions alone (hydrogen rf discharge off), weighted using the dissociation coefficient in the hydrogen beam.

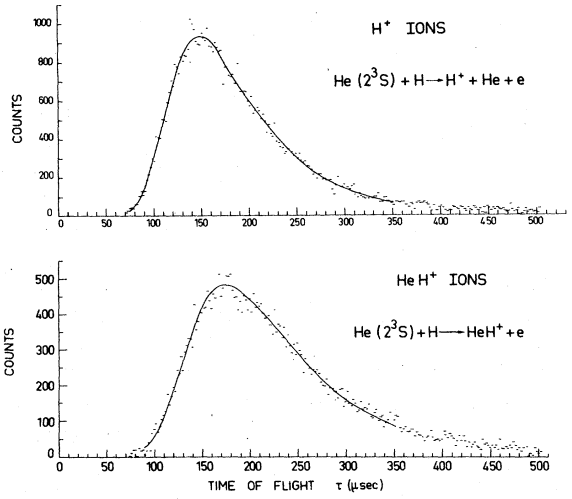

FIG. 2. Time-of-flight spectra of H^+ and HeH^+ ions produced by $He(2\,^3S)$ metastable atoms. The channel width is 2 μsec and the flight path is 46.1 cm. The number of cycles counted is 12×10^6.

B. Determination of the cross sections σ_{AI} and σ_{PI} for $He(2\,^3S) + H$

The same procedure as in our previous paper Ref. 1 is used. In the first step, an effective cross section $\sigma_{eff}(v)$ is obtained as a function of the He* atom velocity v, and then in a second step the real cross section $\sigma(v_r)$ is deduced as a function of the relative velocity v_r of the He* and H colliding particles. The formula used is

$$\sigma(v_r) = v\sigma_{eff}(v)/\bar{v}_r,$$

where $\bar{v}_r$ is the relative velocity averaged over the H target atom velocity distribution. Assuming that $\sigma(v_r)$ depends on v_r^n, we have verified that the average cross section $\langle\sigma(v_r)\rangle$ as a function of $\bar{v}_r$ is equal to the cross section $\sigma(v_r)$ over a range of values of n and T, which includes those of the experiment ($-1 \leq n \leq +3$ and $80\,^\circ\text{K} \leq T \leq 300\,^\circ\text{K}$) within accuracies of 1% when the cross section is a decreasing function of relative velocity ($n < 0$) and 5% when the cross section is a strongly increasing function of relative velocity ($n = 3$).

The velocity dependences of the Penning and associative ionization cross sections are plotted in Fig. 3. The σ_{PI} cross section increases slightly

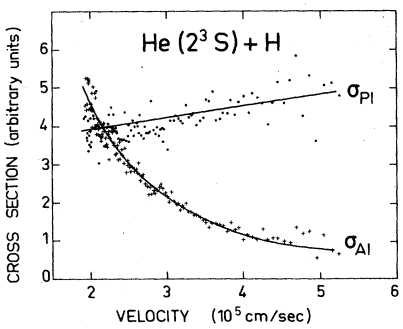

FIG. 3. Penning ionization cross section σ_{PI} and associative ionization cross section σ_{AI} as a function of relative velocity, present experiment (a smooth curve is drawn through the experimental points).

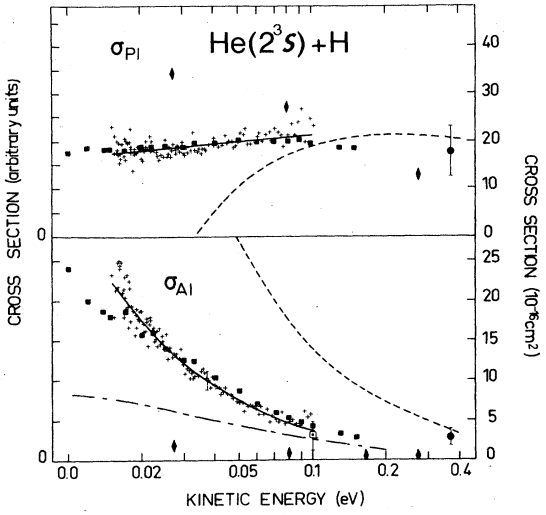

FIG. 4. Penning and associative ionization cross sections for He(2^3S)+H as a function of relative kinetic energy. The solid line with plusses for data points present experiment (as in Fig. 3). These experimental results are relative. The absolute scale has been obtained by normalization to the total cross section σ_{TI} for He(2^3S)+H system calculated at 0.04 eV. ● Experiment, Howard *et al.* (Ref. 11); ⊡ experiment, Magnuson *et al.* (Ref. 12); Dashed line, classical orbiting approximation, Miller *et al.* (Ref. 2) recalculated at low energy (a); Dash-dot-dash line classical theory, Miller *et al.* (Ref. 8) (b); ♦ semiclassical theory, Nakamura (Ref. 4) (a); ■ semiquantum theory, present calculation (a). (a) Counting the decaying molecular ions as dissociated products; (b) counting the decaying molecular ions as associated products.

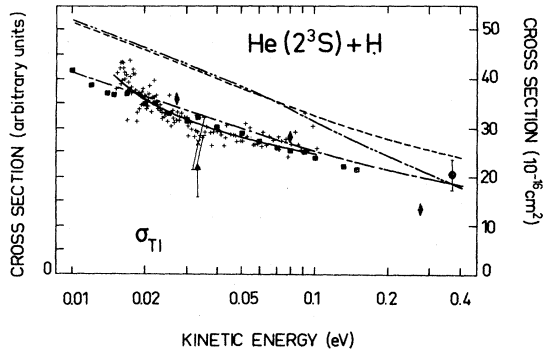

FIG. 5. Total ionization cross section σ_{TI} for He(2^3S)+H as a function of relative kinetic energy. The solid line with plusses for data points, present experiment (as in Fig. 3). These experimental results are relative. The absolute scale has been obtained by normalization to the total cross section σ_{TI} for He(2^3S)+H system calculated at 0.04 eV; ● experiment, Howard *et al.* (Ref. 11); ▲ experiment, Shaw *et al.* (Ref. 10); Dashed line, classical orbiting approximation, Miller *et al.* (Ref. 2) recalculated at low energy; Dash-dot-dash line, classical and semiclassical theory, Miller *et al.* (Ref. 8) and Cohen and Lane (Ref. 6) with V^* from Miller *et al.* (Ref. 2) and $\Gamma_2{}^3{}_S$ from Miller *et al.* (Ref. 8); Dash-double dot-dash line, semiclassical theory, Cohen and Lane (Ref. 5) with V^* from Miller *et al.* (Ref. 2) and $\Gamma_2{}^3{}_S$ from Fujii *et al.* (Ref. 3); ♦ semiclassical theory, Fujii *et al.* (Ref. 3); ✕ theory, Bell (Ref. 7); ■ quantum theory, present calculation.

and monotonically with velocity up to 5200 m/sec while the σ_{AI} cross section decreases strongly (a factor of $\simeq 6$) in the same velocity range. These cross sections are also plotted as a function of relative kinetic energy in Fig. 4.

We have observed that the sum $\sigma_{PI}(v_r)+\sigma_{AI}(v_r)$ as a function of v_r coincides with the total ionization cross section $\sigma_{TI}(v_r)$ resulting from the total ion-production measurement via the Spiralton Bendix 4219X. This confirms the validity of the determination of the spectrum of the H^+ Penning ions. The relative kinetic energy dependence of σ_{TI} is shown in Fig. 5: we note that σ_{TI} decreases by a factor of 1.6 for E_r varying between 0.015 and 0.1 eV.

The ratio $\sigma_{AI}/(\sigma_{AI}+\sigma_{PI})$ is shown in Fig. 6 as a function of relative kinetic energy. This ratio is obtained directly from the two TOF spectra of H^+ and HeH^+ ions, without using the TOF spectrum of He* atoms. Therefore, the accuracy of the ratio is of the same order of magnitude as the one of each cross section. We observe that this ratio decreases with increasing kinetic energy over the range of

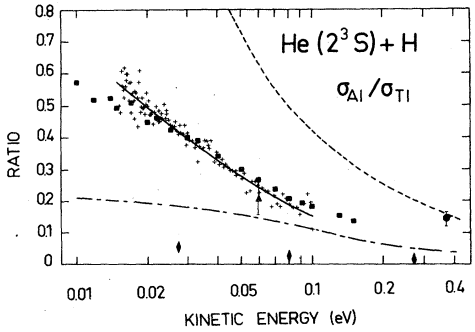

FIG. 6. Ratio σ_{AI}/σ_{TI} as a function of relative kinetic energy. Solid line with plusses for data points, present experiment (as in Fig. 3); ● experiment, Howard *et al.* (Ref. 11); ▲ experiment, deduced from the electron spectrum of Hotop *et al.* (Ref. 22); Dashed line, classical orbiting approximation, Miller *et al.* (Ref. 2) recalculated at low energy (a); Dash-dot-dash line, classical theory, Miller *et al.* (Ref. 8) (b); ◆ semiclassical theory, Nakamura (Ref. 4) (a); ■ semiquantum theory, present calculation (a). (a) Counting the decaying molecular ions as dissociated products; (b) counting the decaying molecular ions as associated products.

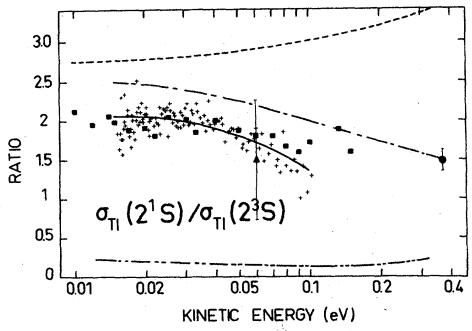

FIG. 7. Ratio $\sigma_{TI}(2^1S)/\sigma_{TI}(2^3S)$ as a function of relative kinetic energy. Solid line with plusses for data points, present experiment (as in Fig. 3); ● experiment, Howard *et al.* (Ref. 11); ▲ experiment, Hotop *et al.* (Ref. 22); Dashed line, classical orbiting approximation, Miller *et al.* (Ref. 2) recalculated at low energy; Dash-dot-dash line, semiclassical theory, Cohen and Lane (Ref. 6) with V^* from Miller *et al.* (Ref. 2) and $\Gamma_{2^1S} = \Gamma_{2^3S}$ from Miller *et al.* (Ref. 8), Dash-double dot-dash line, semiclassical theory, Cohen and Lane (Ref. 5) with V^* from Miller *et al.* (Ref. 2) and Γ from Fujii *et al.*, (Ref. 3); ■ quantum theory, present calculation.

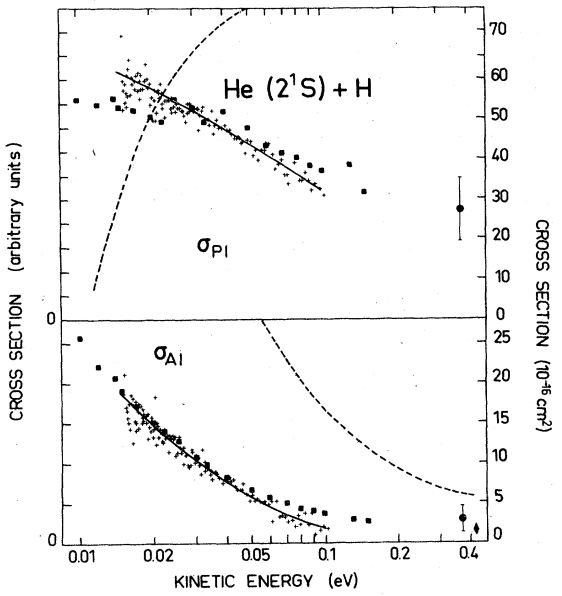

FIG. 8. Penning and associative ionization cross sections for He$(2\,^1S)$ + H as a function of relative kinetic energy. Solid line with plusses for data points, previous experiment (as in Fig. 3.) (Ref. 1). These experimental results are relative. The absolute scale has been obtained by normalization to the total cross section σ_{TI} for He$(2\,^3S)$+ H system calculated at 0.04 eV,; ● experiment, Howard *et al.* (Ref. 11); Dashed line, classical orbiting approximation, Miller *et al.* (Ref. 2) recalculated at low energy (a); ♦ semiclassical theory, Nakamura (Ref. 4) (a); ■ semiquantum theory, present calculation (a), (a) counting the decaying molecular ions as dissociated products.

experimental measurements by a factor of 3.7, and that at the lowest energy involved (0.015 eV) the ratio reaches values as high as 50%.

C. Determination of the cross sections σ_{AI} and σ_{PI} for He(2^1S) + H

By making measurements with and without the quenching helium discharge lamp, we obtain cross sections for He$(2\,^1S)$ + H and for He$(2\,^3S)$ + H separately.

The experimental ratio $\sigma_{T_I}(2\,^1S)/\sigma_{T_I}(2\,^3S)$ is derived after measurements of the ratio of the singlet component to the triplet component of the metastable beam (the TOF spectra of the two metastable species are similar). For our experimental conditions in the metastable atom source (600 mA, 100 V, 0.15 torr), the ratio is found to be He$(2\,^1S)$/He$(2\,^3S) = 1.6$. Here we have assumed that the electron multiplier detecting He* atoms is sensitive to the flux of atoms, and that the secondary emission coefficients γ of the CuBe first dynode are such that $\gamma(2\,^1S)/\gamma(2\,^3S) = 0.81$.[15] The ratio $\sigma_{T_I}(2\,^1S)/\sigma_{T_I}(2\,^3S)$ is plotted in Fig. 7, and we observe that it reaches values as high as 2.

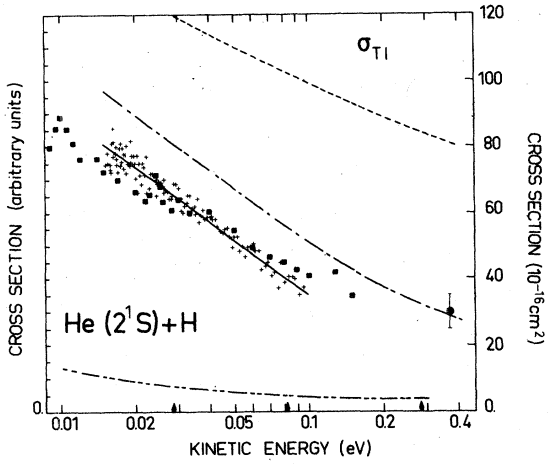

FIG. 9. Total ionization cross section σ_{TI} for He$(2\,^1S)$ + H as a function of relative kinetic energy. Solid line with plusses for data points previous experiment (as in Fig. 3). (Ref. 1); These experimental results are relative. The absolute scale has been obtained by normalization to the total cross section σ_{TI} for He(2^3S)+ H system calculated at 0.04 eV. ● experiment, Howard *et al.* (Ref. 11); Dashed line, classical orbiting approximation, Miller *et al.* (Ref. 2) recalculated at low energy; Dash-dot-dash line, semiclassical theory, Cohen and Lane (Ref. 6) with V^* from Miller *et al.* (Ref. 2) and $\Gamma_{2^1S} = \Gamma_{2^3S}$ from Miller *et al.* (Ref. 8), Dash-double-dot-dash line, semiclassical theory, Cohen and Lane (Ref. 5) with V^* from Miller *et al.* (Ref. 2) and Γ from Fujii *et al.* (Ref. 3); ♦ semiclassical theory Fujii *et al.* (Ref. 3); ■ quantum theory present calculation.

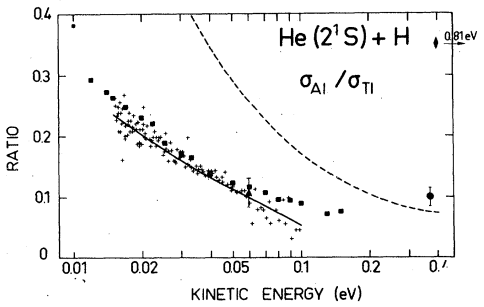

FIG. 10. Ratio σ_{AI}/σ_{TI} for He($2\,^1S$) as a function of relative kinetic energy. Solid line with plusses for data points, previous experiment (as in Fig. 3) (Ref. 1); ● experiment, Howard *et al.* (Ref. 11); ▲ experiment, deduced from the electron spectrum of Hotop *et al.* (Ref. 22); Dashed line classical orbiting approximation, Miller *et al.* (Ref. 2) recalculated at low energy (a); ■ semi-quantum theory, present calculation (a).
(a) Counting the decaying molecular ions as dissociated products.

The experimental velocity dependences of the cross sections σ_{AI}, σ_{PI}, and σ_{TI} are similar to those described in our previous paper.[1] For further comparison with theory they are shown in Fig. 8 (σ_{AI} and σ_{PI}), Fig. 9 (σ_{TI}), and Fig. 10 (σ_{AI}/σ_{TI}).

IV. THEORETICAL APPROACH

The classical or semiclassical Jeffreys-Wentzel-Kramers-Brillouin (JWKB) treatment of the He* + H system is expected to fail because the well depths [0.4 eV for He($2\,^1S$) + H and 1.8 eV for He($2\,^3S$) + H] are much larger than the kinetic energy of the system (0.015–0.1 eV).

The criterion of validity of the JWKB approximation is $d\lambda\!\!\!^{-}/dR \ll 1$, where $\lambda\!\!\!^{-}$ is the generalized de Broglie wavelength of the system. In the first approximation where the autoionization width $\Gamma(R)$ is small compared to the incoming channel potential $V^*(R)$, $\lambda\!\!\!^{-}$ is given by

$$\lambda\!\!\!^{-} = \hbar/\{2\mu\,[E_c - V^*(R)] - l(l+1)/R^2\}^{1/2},$$

where E_c is the initial relative kinetic energy of He* + H and μ is the reduced mass of the system. If $\lambda\!\!\!^{-}$ and consequently $V^*(R)$ varies only slightly with R, the system is close to being classical. This may be true for the singlet, but it is not for the triplet where the repulsive wall of V^* is much steeper than in the singlet case. Anyhow, in both singlet and triplet cases, at the turning point R_0 $\lambda\!\!\!^{-} \to \infty$ and the accuracy of the JWKB approximation breaks down. Therefore, an accurate calculation of the ionization cross sections requires a quantum resolution of the Schrödinger equation.

A. Numerical solution of the Schrödinger equation

The radial Schrödinger equation describing the relative motion of the particles is[16]

$$\left[\frac{d^2}{dR^2} + \frac{2v}{\hbar^2}\left(E_c - V^*(R) + \frac{i}{2}\Gamma(R)\right) - \frac{l(l+1)}{R^2}\right] v_l(R) = 0, \tag{1}$$

where $v_l(R)$ is a complex wave function. The real and imaginary parts

$$v_{1l}(R) + i v_{2l}(R) = v_l(R) \tag{2}$$

satisfy the system of equations

$$\left(\frac{d^2}{dR^2} + \frac{2v}{\hbar^2}[E_c - V^*(R)] - \frac{l(l+1)}{R^2}\right)\begin{pmatrix} v_{1l}(R) \\ v_{2l}(R)\end{pmatrix} = \frac{\mu}{\hbar^2}\begin{pmatrix} 0 & \Gamma(R) \\ -\Gamma(R) & 0\end{pmatrix}\begin{pmatrix} v_{1l}(R) \\ v_{2l}(R)\end{pmatrix}. \tag{3}$$

Instead of using the Numerov or Runge-Kutta method to solve the coupled equations, we have generalized the method described in Ref. 17 to the case of a differential system. The interest of this method is its easy programming and its short computing time.

The wave functions $v_{1l}(R)$ and $v_{2l}(R)$ are generated step by step (a step of 0.01 a.u. is satisfying), and they satisfy the regularity condition at $R = 0$. At large value of R, amplitudes and phase shifts converge rapidly towards the values A_{il} and δ_{il}. The asymptotic expression for the wave function is therefore

$$v_{il}(R) \underset{R\to\infty}{\sim} A_{il}\sin(kR - \tfrac{1}{2}l\pi + \delta_{il}), \quad i = 1,2 \tag{4}$$

which can be written as a linear combination of spherical Bessel and Neumann functions

$$v_{il}(R) \underset{R\to\infty}{\sim} A_{il}kR\,[j_l(kR)\cos\delta_{il} - n_l(kR)\sin\delta_{il}]. \tag{5}$$

Amplitudes A_{il} and phase shifts δ_{il} are deduced from the position R^0_{il} of the zeros and R^m_{il} of the maxima of the asymptotic expression of $v_{il}(R)$ given by formula (5). They are, respectively,

$$A_{il} = \frac{v_{il}(kR^m_{il})}{kR^m_{il}\,[j_l(kR^m_{il})\cos\delta_{il} - n_l(kR^m_{il})\sin\delta_{il}]}, \tag{6}$$

$$\delta_{il} = \arctan[j_l(kR^0_{il})/n_l(kR^0_{il})]. \tag{7}$$

B. Total ionization cross section σ_{TI}

It is convenient to introduce the $\underline{R}$ matrix

$$v_l(R) \underset{R\to\infty}{\sim} \sin(kR - \tfrac{1}{2}l\pi) + \underline{R}_l\cos(kR - \tfrac{1}{2}l\pi), \tag{8}$$

which gives by identification with formula (4)

$$\underline{R}_l = \frac{A_{1l}\sin\delta_{1l} + iA_{2l}\sin\delta_{2l}}{A_{1l}\cos\delta_{1l} + iA_{2l}\cos\delta_{2l}} . \quad (9)$$

Introducing formulas (6) and (7) into formula (9) gives the $\underline{R}_l$ elements of the $\underline{R}$ matrix. The real and imaginary parts are, respectively,

$$\mathrm{Re}\underline{R}_l = \frac{A_{1l}^2 \sin\delta_{1l}\cos\delta_{1l} + A_{2l}^2 \sin\delta_{2l}\cos\delta_{2l}}{A_{1l}^2\cos^2\delta_{1l} + A_{2l}^2\cos^2\delta_{2l}}, \quad (10)$$

$$\mathrm{Im}\underline{R}_l = \frac{A_{1l}A_{2l}(\sin\delta_{2l}\cos\delta_{1l} - \sin\delta_{1l}\cos\delta_{2l})}{A_{1l}^2\cos^2\delta_{1l} + A_{2l}^2\cos^2\delta_{2l}} . \quad (11)$$

The total ionization cross section is obtained from

$$\sigma_{TI} = \frac{\pi}{k^2}\sum_l (2l+1)(1 - |S_l|^2), \quad (12)$$

where the $\underline{S}$ matrix is connected to the $\underline{R}$ matrix by

$$\underline{S}_l = (1 + i\underline{R}_l)/(1 - i\underline{R}_l) , \quad (13)$$

in which we introduce formulas (10) and (11).

Calculation of σ_{TI} is carried out via formula (12) with $V^*(R)$ and $\Gamma(R)$ as defined in Secs. IV D and IV E, respectively, for both systems $He(2\,^3S) + H$ and $He(2\,^1S) + H$.

C. Associative ionization cross section σ_{AI}

The Schrödinger equation (1) is solved by the same method as in the case of σ_{TI}: the only difference between the σ_{AI} and σ_{TI} calculations is that $\Gamma_{AI}(R)$ replaces $\Gamma(R)$ in formulas (1) and (3). The coupling width $\Gamma_{AI}(R)$ is defined via the classical criterion[4]:

$$R > R_{AI}, \quad \Gamma_{AI}(R) = 0 ,$$
$$R < R_{AI}, \quad \Gamma_{AI}(R) = \Gamma(R). \quad (14)$$

Thus, the coupling width $\Gamma_{AI}(R)$ is extended over the truncated range of R $(R < R_{AI})$; beyond R_{AI} only the real part $V^*(R)$ of the complex potential is kept. The wave function $v_l(R)$, amplitudes A_{il} and phase shifts δ_{il} leading to the $\underline{R}$ and $\underline{S}$ matrix are calculated numerically as for σ_{TI}.

The determination of R_{AI} is based on the conservation of total energy of the colliding system, as is done in the classical theoretical approach for the $He^* + Ar$ in Ref. 14. As the excess potential energy is carried away by the ejected electron, its kinetic energy is

$$\epsilon(R) = V^*(R) - V^+(R), \quad (15)$$

where $V^*(R)$ and $V^+(R)$ are the incoming- and outgoing-channel potential curves. The conservation of total energy is written

$$E_c^+ = E_c + V^*(\infty) - \epsilon(R) , \quad (16)$$

where E_c is the relative kinetic energy of $He^* + H$, and $V^+(\infty)$ is taken as zero, and E_c^+ is the relative kinetic energy of $He + H^+$. R_{AI} is defined as the critical value such that

$$E_c^+(R_{AI}) = 0. \quad (17)$$

If $E_c^+(R_{AI}) > 0$, an H^+ ion is produced, i.e., Penning ionization takes place. If $E_c^+(R) < 0$, a bound state HeH^+ is created, i.e., associative ionization takes place. Formula (17) rather than formula

$$E_c^+(R_{AI}) = E_m \quad (18)$$

(where E_m is the secondary maximum of the $He + H^+$ potential curve resulting from the centrifugal term) has been used, because in the experiment the ions are detected several microseconds after being created. Thus, most of the HeH^+ ions produced in the range $\{R_{AI}[E_c^+(R_{AI}) = 0],\ R_{AI}[E_c^+(R_{AI}) = E_m]\}$ have enough time to dissociate by tunneling.

This approach to σ_{AI} enabled us to save computing time compared with the pure quatum σ_{AI} calculation which requires the final wave function in all the vibrational states of HeH^+. However, we stress that it is approximative in that it neglects the "survival factor" which appears in classical formulation.

D. Data

The total ionization cross section σ_{TI} given by Eq. (12) is seen to be a function only of $V^*(R)$ and $\Gamma(R)$, while the associative ionization is seen to be a function of $V^*(R)$ and $\Gamma(R)$, plus $V^+(R)$ via formula (17).

The incoming-channel potential curves calculated by Miller *et al.* (MS),[2] which seem more trustworthy than the ones calculated by Fujji *et al.*,[3] are used in our calculations. An analytical form being convenient, a least-squares routine was used to obtain the best fit of a Morse potential in the well and a screened Van der Waals potential beyond the well, to the ten values of $V^*(R)$ calculated in Ref. 2 in the range $2 \leq R \leq 10$ a.u.

As a quantum calculation of the cross sections is performed in the present work, the range of R is not bounded by the turning point R_0 (which is always larger than 2.2 a.u. for $He^* + H$). In order to obtain good accuracy in the calculation it has been necessary to extend slightly the potential curves beyond 2 a.u.. Over this short-range region of R, we have used an inverse power potential.

The analytical form is

$$V^*(R) = C_1/R^2 - C_2, \quad R_1 < R < R_2$$
$$V^*(R) = \epsilon[e^{2\alpha(1-R/Re)} - 2e^{\alpha(1-R/Re)}], \quad R_2 \leq R \leq R_3 \quad (19)$$
$$V^*(R) = -C_6[1 + (B + CR + DR^2)e^{-AR}]/R^6, \quad R > R_3 .$$

TABLE I. Values of the parameters in the analytic forms of the potential curves $V^*(R)$ for $He(2^1S)+H$ $He(2^3S+H$ and $V^+(R)$ for $He+H^+$.

Parameter (a.u.)	$He(2^1S)+H$	$He(2^3S)+H$	$He+H^+$
C_1	0.0778094	0.971967	
C_2	0.075554	0.184873	
ϵ	0.014098	0.06935	
α	2.0611	1.9969	1.3835
Re	5.5434	3.5015	
C_6	135	85	
A	1.60	0.80	0.442
B	$8.444353\times10^{+7}$	$9.5376\times10^{+3}$	0.505
C	$-2.54779\times10^{+7}$	$-4.3452\times10^{+3}$	0.451
D	$1.93\times10^{+8}$	504.0	
W			4.37311
R_1	1.3	0.8	
R_2	2.5	2.0	
R_3	7.0	5.0	

The potential parameters are tabulated in Table I.

The HeH^+ potential has been represented by an analytic function by Helbig *et al.*,[18]

$$V^+(R)=\frac{2}{R}e^{-R/A}\left[1+\frac{R}{A}+\frac{R^2}{2}\left(\frac{1}{A^2}-\frac{W}{B}\right)\right]$$
$$-W\left[1+\frac{R}{B}+\frac{R^2}{C^2}+\frac{2WR^4}{\alpha}\right]. \quad (20)$$

The parameters have been determined by these authors so as to have a reasonable agreement with the Born-Oppenheimer energies calculated by Michels[19] and to pass through the value −0.075 Hartree at its minimum in accord with the accurate variational calculation of Wolniewicz.[20] The values of the parameters are given in Table I.

E. Results for the $He(2^3S)+H$ system

1. *Cross-section ratio. Determination of the width for triplet* $\Gamma_{2^3S}(R)$

As in our previous classical interpretation of $He(2^3S)+Ar$,[14] the σ_{AI}/σ_{TI} ratio is used to determine the remaining unknown parameters, which here correspond to $\Gamma_{2^3S}(R)$.

We note that Miller *et al.* (MSS)[8] have calculated σ_{AI} and σ_{TI} classically by using the four values of Γ_{2^3S} obtained by MS,[2] where σ_{AI} contains all of the resonance states of HeH^+ bound in the effective radial potential, and where R_{AI} is defined by Eq. (18). On the other hand the interpretation of our experiment determines R_{AI} via Eq. (17). It follows that if we calculate σ_{AI}/σ_{TI} just as in MSS[8] but using Eq. (17) then the result will be smaller than in MSS (0.2 for 0.15 eV). The latter is already smaller than the experimental result (0.5 for 0.15 eV). We have tried to find a coupling width $\Gamma_{2^3S}(R)$ which is as close as possible to the four values for $\Gamma(R)$ calculated by MS[2] for the $He(2^3S)+H$ system and simultaneously consistent with our experimental σ_{AI}/σ_{TI} ratios. We have succeeded in using an exponential form as was previously proposed by Bates *et al.*[21] The parameters A and B of $\Gamma_{2^3S}(R)=Ae^{-R/B}$ are those giving the best least-squares fit to the four values of Γ given in MS[2] for $He(2^3S)+H$. They are equal to

$$A=0.05248 \text{ a.u.}, \quad B=0.9566 \text{ a.u.} \quad (21)$$

$\Gamma_{2^3S}(R)$ as a function of R is plotted in Fig. 11, and compared to the width obtained by MS.[2] Nineteen values of σ_{AI}/σ_{TI} corresponding to energies be-

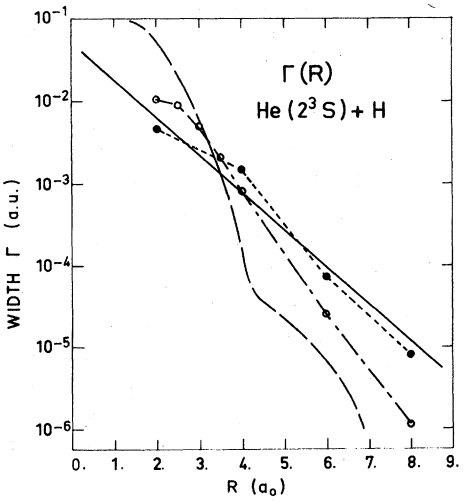

FIG. 11. Autoionization width $\Gamma(R)$ for $He(2^3S)+H$. Continuous line, present work; Double-dash line, Bell (Ref. 7); ● Miller *et al.* (Ref. 8); ○ Hickman *et al.* (Ref. 9).

tween 0.01 and 0.15 eV have been calculated by our method and they are shown in Fig. 6. They provide a good description of the experimental ratio over the range 0.015–0.10 eV.

2. *Cross sections*

The 19 values of the Penning ionization cross section σ_{PI} and of the associative ionization cross section σ_{AI} calculated with criterion (17) are plotted in Fig. 4. Our experimental results are relative; the choice of the parameters A and B of Γ_{2^3s} leads to absolute values of the cross sections, referenced on the absolute scale which is given on the right-hand side of each figure. Our experimental total ionization cross section σ_{TI} has been normalized to our theoretical cross section at around 0.04 eV energy for which the dispersion of the experimental points is the smallest. The σ_{TI} theoretical values are plotted on Fig. 5. A very good agreement between the theory and experiment is observed.

F. Results for the He(2^1S) + H system

1. *Cross-section ratios–determination of the width for singlet* $\Gamma_{2^1S}(R)$

The ratios $\sigma_{TI}(2^1S)/\sigma_{TI}(2^3S)$ and σ_{AI}/σ_{TI} for He(2^1S) + H have been obtained experimentally. Knowing these two ratios enable us to determine $\Gamma_{2^1S}(R)$. This later has been found varying exponentially with R as was $\Gamma_{2^3S}(R)$ and the parameters A' and B' such that $\Gamma_{2^1S}(R) = A'e^{-R/B'}$ are equal to $A' = A/1.04$ and $B' = B$, where A and B are the parameters of $\Gamma_{2^3S}(R)$ given by formula (21). We can therefore conclude that the approximation $\Gamma_{2^1S} = \Gamma_{2^3S}$ used by Cohen and Lane[6] was not so crude as we previously suggested.[1] The nineteen calculated values of $\sigma_{TI}(2^1S)/\sigma_{TI}(2^3S)$ and of σ_{AI}/σ_{TI} are plotted in Figs. 7 and 10.

2. *Cross sections*

The absolute values of the cross sections for He(2^1S) results from the normalization of our experimental σ_{TI} for He(2^3S) + H. The values of σ_{AI}, σ_{PI}, and of σ_{TI} are shown, respectively, in Figs. 8 and 9.

While we satisfactorily reproduce the experimental data on σ_{AI}, we can observe in our calculations of σ_{PI} a jump at 0.025 eV. This phenomenon is reflected in the calculated values of σ_{TI}, and of the ratios σ_{AI}/σ_{TI}, and $\sigma_{TI}(2^1S)/\sigma_{TI}(2^3S)$. In order to clarify this point, we have calculated eight more values of σ_{TI} in the low-energy portion. We then find peaks in the calculated values at 0.010 and 0.024 eV. Each peak is generated by one partial wave with high orbital angular momentum l and the corresponding partial cross section σ_l takes a high value. At 0.01 eV, the orbital momentum as 13 and at 0.024 eV it is $l = 19$. This phenomenon is typical of orbiting.

V. DISCUSSION

A. Error analysis

A possible source of errors is the determination of the zeros of the time scales of the TOF spectra. Two determinations are necessary: the zero of the He* TOF spectrum time scale and the zero of the ion TOF spectrum time scales. An error of 1 or 2 μsec (the channel width) is possible, resulting in an uncertainty in the He* velocity v of less than 2%. Because the ratios σ_{AI}/σ_{TI} and $\sigma_{TI}(2^1S)/\sigma_{TI}(2^3S)$ are obtained without using the He* TOF spectrum, this error does not affect their values, while such an error in the relative position of the zeros of the two time scales of He* and ions would result in uncertainties in the value of the cross sections of the order of 10%. The dispersion of the points in Figs. 3–10 illustrates the precision of the measurements. In the case of $\sigma_{PI}(2^3S)$, $\sigma_{TI}(2^3S)$, and $\sigma_{AI}/\sigma_{TI}(2^3S)$, one has to take into account in addition, the precision of the measurement of the transmission modification (see Sec. II) which is 10%. In the case of σ_{AI}, an additional uncertainty $\leq 5\%$ is introduced as a consequence of subtracting two TOF spectra using the dissociation coefficient (see Sec. III A).

Calculations of cross sections are extended to value of l such that the precision on the amplitude A_{il} and the phase shift δ_{il} is better than 10^{-4} ($\Delta A_{il}/A_{il} = \Delta\delta_{il}/\delta_{il} \simeq 10^{-4}$). The resulting cross-section precision is $\Delta\sigma/\sigma \simeq 5.10^{-2}$. The number of angular momenta l taken into account is never more than 60.

B. Experiment

Until now the measurements of σ_{TI} made in other laboratories have been carried out without velocity selection and were consequently averages over the velocity distributions of the colliding atoms. This is the case for the $\sigma_{TI}(2^3S)$ of Shaw *et al.*[10] obtained in a flowing afterglow at 300 °K, which is found to lie below our result (see Fig. 5), and for σ_{TI}, σ_{PI}, and σ_{AI} (2^1S and 2^3S) of Howard *et al.*[11] at 0.37 eV. Since this energy is located outside of our range of measurement, we can only say that the points of Howard *et al.* seem consistent with the extrapolation of our cross sections (see Figs. 4, 5, 8, and 9).

The only measurement for which the relative kinetic energy is well defined concerns $\sigma_{AI}(2^3S)$ made by Magnuson *et al.*[12] in a merging beam set up at 0.1 eV; a second measurement was carried out at 1 eV but does not appear on our figures (see Fig.

4). The other points given in Ref. 12 are for deuterium. The agreement between our cross section $\sigma_{AI}(2\,^3S)$ and that of Magnuson *et al.* is very good.

The values of σ_{AI}/σ_{TI} for $He(2\,^3S)+H$ reach 52% at 0.015 eV (Fig. 6) which is much larger than the 24% reached by σ_{AI}/σ_{TI} for $He(2\,^1S)+H$ shown in Fig. 10. As in Ref. 1, we have deduced from the Penning electron spectrum of Hotop *et al.*[22] a value of σ_{AI}/σ_{TI} for $He(2\,^3S)+H$ at 0.06 eV which is in agreement with our curve. These ratios point out the large difference between the $He(2\,^3S)+H$ system and the $He(2\,^1S)+H$ system. The origin of this distinction is the quite different well depths of the two incoming-channel potentials since the widths $\Gamma_{2\,^1S}$ and $\Gamma_{2\,^3S}$ are nearly the same. This difference is also evident in the $\sigma_{TI}(2\,^1S)/\sigma_{TI}(2\,^3S)$ ratio which reaches 2.2 at 0.015 eV. The value published by Hotop *et al.* at 0.06 eV is slightly smaller than ours.

C. Theory

It can be seen on Figs. 4, 5, 8, and 9 that in any case, the classical orbiting approximation cannot provide a satisfactory interpretation of Penning processes. At low energies we have recalculated the cross sections σ_{AI}, σ_{PI}, and σ_{TI} for $He(2\,^1S)$ and $He(2\,^3S)$ with the orbiting formulas of MS.[2] A general overestimation is observed for σ_{AI} and σ_{TI} in the $He(2\,^3S)$ and $He(2\,^1S)+H$ systems; for σ_{PI}, even the energy dependence is different from that of the experimental curve. However this simplified model is interesting because the formulas giving σ_{TI} and σ_{AI} can be formally inverted in a simple way and lead to $V^*(R)$ and $V^+(R)$. But its inadequacy appears clearly on Figs. 6 and 10 where we represent the σ_{AI}/σ_{TI} ratios which have the advantage of eliminating the problems of the absolute value of the cross sections [except the values of the secondary emission coefficients $\gamma(2\,^1S)$ and $\gamma(2\,^3S)$]. However we do not question the potential $V^*(R)$ which was calculated by MS[2] and which we used.

By a semiclassical method, Fujii *et al.*[3] and Nakamura[4] calculated σ_{TI} and σ_{AI} cross sections, respectively, from the potentials $V^*(R)$ and widths $\Gamma(R)$ calculated in Ref. 3. A satisfactory agreement is observed in the $He(2\,^3S+H)$ case with our σ_{TI} cross section (see Fig. 5) while in the $He(2\,^1S)+H$ case, their σ_{TI} cross section is much smaller than ours. Their $He(2\,^1S)+H$ potential curve, which shows a pure repulsive shape, seems to be too far from reality. Let us note that the $He(2\,^1S)+H$ potential curve calculated by MS,[2] has a well depth of 0.4 eV; in the case of $He(2\,^3S)+H$, the well depth of $V^*(R)$ calculated by Fujii *et al.*[3] is 1.1 eV while the one calculated by MS[2] is 1.8 eV.

In 1972, Miller, Slocomb, and Schaefer (MSS)[8] used a classical method to derive the σ_{AI} and σ_{TI} cross sections for $He(2\,^3S)+H$ system, after having calculated the corresponding width $\Gamma_{2\,^3S}(R)$. They used the potential of MS[2] and the same criterion as Nakamura[4] to define R_{AI}. The agreement between their results and ours is limited to σ_{TI} (see Fig. 5); their σ_{AI} cross section is smaller than ours, by a factor of 2 at 0.03 eV (see Figs. 4 and 6). Furthermore, they include in σ_{AI} all the decaying molecular ions bound in the rotational barrier of the effective HeH^+ potential, while in our experiment they have enough time to dissociate before being detected. Then the corresponding σ_{AI} would be still smaller than the previous one. No results have been published on σ_{AI} for $He(2\,^1S)+H$ in our kinetic-energy range.

In 1973, Cohen and Lane[6] used the potentials of MS[2] and the width $\Gamma_{2\,^3S}$ of MSS[8] for $He(2\,^3S)+H$ and $He(2\,^1S)+H$. Their approximation of $\Gamma_{2\,^1S}$ by $\Gamma_{2\,^3S}$ was not drastic as can be seen by the fact that we obtain here $\Gamma_{2\,^1S}=\Gamma_{2\,^3S}/1.04$. By a semiclassical JWKB method they obtained the σ_{TI} cross sections, and in the case of $He(2\,^3S)+H$ the agreement with our σ_{TI} cross section is good (see Fig. 4). However in the case of $He(2\,^1S)+H$, the agreement is limited to the energy dependence, the absolute value being about 20% higher than ours (see Fig. 9). This difference can also be seen for the $\sigma_{TI}(2\,^1S)/\sigma_{TI}(2\,^3S)$ ratio in Fig. 7.

The absence of results for $\sigma_{AI}(2\,^1S)$ and the lack of harmony between $\sigma_{AI}(2\,^3S)$ of MSS[8] and our experimental data encouraged us to find a numerical solution of the Schrödinger equation with a complex potential $V^*(R)-\frac{1}{2}i\Gamma(R)$. The calculation of the associative cross sections σ_{AI}, using a truncated width neglects the survival factor which appears in the classical approach of Miller.[23] In order to point out the influence of the neglect of the survival factor we calculated the Penning ionisation cross sections σ_{PI} with a truncated width $\Gamma_{PI}(R)$ replacing $\Gamma(R)$ in formulas (1) and (3). The coupling width $\Gamma_{PI}(R)$ is defined via the classical criterion.

$$R>R_{AI},\quad \Gamma_{PI}(R)=\Gamma(R),$$
$$R<R_{AI},\quad \Gamma_{PI}(R)=0. \tag{22}$$

The comparison between the values of the total cross sections obtained by $\sigma_{PI}+\sigma_{AI}$ and the values of the total cross sections σ_{TI} obtained directly (Sec. IV B) gives us an upper limit for the error due to the neglect of the survival factor. The $\sigma_{PI}+\sigma_{AI}$ cross sections are higher than σ_{TI} cross sections. This effect causes an overestimate of σ_{AI}: the upper limit for the error is 11% at 0.015 eV and 4%

at 0.1 eV for the singlet, and 20% at 0.015 eV and 10% at 0.1 eV for the triplet.

In order to underline the effect of the shape of the width $\Gamma(R)$ on the cross section we have calculated σ_{TI} and σ_{AI} using the classical formulas of Miller[23] with the partition of $\Gamma(R)$ into $\Gamma_{PI}(R)$ and $\Gamma_{AI}(R)$ on both sides of R_{AI}, R_{AI} being defined as in Sec. IV C.

$$\sigma_{TI} = 2\pi \int_0^\infty b\, db \left[1 - \exp\left(-2 \int_{R_0}^\infty \frac{\Gamma(R)\, dR}{\hbar V_b(R)}\right)\right], \quad (23)$$

$$\sigma_{AI} = 4\pi \int_0^\infty b\, db \exp\left(- \int_{R_0}^\infty \frac{\Gamma(R)\, dR}{\hbar V_b(R)}\right) \times \sinh \int_{R_0}^{R_{AI}} \frac{\Gamma(R)\, dR}{\hbar V_b(R)} . \quad (24)$$

We have introduced in formulas (23) and (24) the R_{AI} criterion of Miller [decaying molecular ions included in σ_{AI} formula (18)] and the same data for $V^*(R)$, $V^+(R)$, and $\Gamma(R)$ as we used in Sec. IV of the present paper formulas (19), (20), and (21). We have therefore obtained a total ionization cross section $\sigma_{TI}(2\,^3S)$ equal to within 5% the $\sigma_{TI}(2\,^3S)$ of MSS,[8] while the associative ionization cross section $\sigma_{AI}(2\,^3S)$ is larger than MSS's one by factors of 1.6 at 0.015 eV and 1.35 at 0.1 eV. This fact is not surprising, the σ_{AI} cross section being more sensitive than σ_{TI} cross section to transition taking place at short range. In order to point out the difference between our semiquantum calculation and classical results we calculated the classical cross sections σ_{TI} formula (23) and σ_{AI} formula (24) with our R_{AI} criterion [decaying moleculaire ions dissociating before detection formula (17)] and with the same data for $V^*(R)$, $V^+(R)$, and $\Gamma(R)$ as we used in Sec. IV formulas (19)–(21). We obtained the classical total ionization cross section $\sigma_{TI}(2\,^3S)$ and $\sigma_{TI}(2\,^1S)$ equal to our calculated cross section, but the classical associative ionization cross section $\sigma_{AI}(2\,^3S)$ and $\sigma_{AI}(2\,^1S)$ are lower than our estimation 35% smaller at 0.015 eV and 25% smaller at 0.1 eV for $\sigma_{AI}(2\,^3S)$ and only 15% smaller at 0.015 eV for $\sigma_{AI}(2\,^1S)$.

A very recent calculation of Hickman *et al.*[24] has been carried out in the classical framework. They reproduce exactly our experimental ratio σ_{AI}/σ_{TI} for $He(2\,^1S)+H$ after having calculated Γ_{2^1S}. By using their Γ_{2^3s} previously published,[9] they calculate the ratio σ_{AI}/σ_{TI} for $He(2\,^3S)+H$ which is found 40% and 20% smaller than our experimental ratio at 0.02 and 0.10 eV, respectively.

APPENDIX: RESULTS ON D

We have measured the Penning and associative ionization cross sections for $He(2^1S)+D$ and $He(2^3S)+D$. The experimental conditions were the same as in the hydrogen measurements. The only difference was that we found that the dissociation coefficient of deuterium measured in the beam was higher than in the case of hydrogen and so the experiment was easier to run.

Since our experimental results are relative, we cannot obtain the value of the ratio of the Penning ionization cross sections for D and H. However we observed that this ratio, describing the isotope effect, is constant over the energy range considered.

We have calculated quantum mechanically these cross sections, with the same data as were used in Sec. IV for He^*+H. We have observed that the energy dependences of the cross section for D and H are similar on the whole, although the calculated points do not coincide exactly. It appears that the isotope effects are slightly different for the triplet and singlet systems, 1.1 and 1.2, respectively.

In a previous work[25] we derived the σ_{PI} cross section for $He(2\,^1S)+D$, via the Berkling correction formula to deduce $\sigma(v_r)$ from the experimental effective cross section $\sigma_{eff}(v)$. In the present work this step has been completely modified and improved as described in Sec. III B. The $\sigma_{PI}(2\,^1S)$ cross section observed in Ref. 25 is found to be slightly flatter than the one obtained here, but is nonetheless consistent with the theoretical values.

The works of Neynaber and Magnuson[12,26] study σ_{AI}, σ_{PI}, and σ_{TI} in the 0.1–10-eV energy range. Their energy range is located just outside of our range of measurements; thus, we can only say that their σ_{PI} cross section exhibits a decrease with increasing energies not consistent with the extrapolation of our cross section, while a good agreement is observed for σ_{AI} for which one extra value at 0.05 eV lies in the energy range which we studied.

ACKNOWLEDGMENT

The authors wish to acknowledge Dr. H. Nakamura and Dr. C. Manus for helpful discussions.

*Present address: Onera-29, Avenue Division Leclerc 92, Chatillon sous Bagneux, France.

[1] J. Fort, J. J. Laucagne, A. Pesnelle, and G. Watel, Phys. Rev. A 14, 658 (1976).

[2] W. H. Miller and H. F. Schaefer, J. Chem. Phys. 53, 1421 (1970).

[3] H. Fujii, H. Nakamura, and M. Mori, J. Phys. Soc. Jpn. 29, 1030 (1970).

[4]H. Nakamura, J. Phys. Soc. Jpn. 31, 574 (1971).
[5]J. S. Cohen and N. F. Lane, Chem. Phys. Lett. 10, 63 (1971).
[6]J. S. Cohen and N. F. Lane, J. Phys. B 6, L113 (1973).
[7]K. L. Bell, J. Phys. B 3, 1308 (1970).
[8]W. H. Miller, C. A. Slocomb, and H. F. Schaefer, J. Chem. Phys. 56, 1347 (1972).
[9]A. P. Hickman, A. D. Isaacson, and W. H. Miller, J. Chem. Phys. 66, 1483 (1977).
[10]M. J. Shaw, R. C. Bolden, R. S. Hemsworth, and N. D. Twiddy, Chem. Phys. Lett. 8, 148 (1971).
[11]J. S. Howard, J. P. Riola, R. D. Rundel, and R. F. Stebbings, J. Phys. B 6, L109 (1973).
[12]G. D. Magnuson and R. H. Neynaber, J. Chem. Phys. 60, 3385 (1974).
[13]A. Pesnelle, A. Hourdin, G. Watel, and C. Manus, J. Phys. B 6, L326 (1973).
[14]A. Pesnelle, G. Watel, and C. Manus, J. Chem. Phys. 62, 3590 (1975).
[15]F. B. Dunning, R. D. Rundel, and R. F. Stebbings, Rev. Sci. Instrum. 46, 697 (1975).
[16]N. F. Mott and H. S. W. Massey, *The Theory of Atomic Collisions* (Oxford, London, 1965), Chap. VIII, Sec. 2.
[17]R. de Vogelaere, J. Res. Natl. Bur. Stand. (U.S.) 54, 3 (1955).
[18]H. F. Helbig, D. B. Millis, and L. W. Todd, Phys. Rev. A 2, 771 (1970).
[19]H. H. Michels, J. Chem. Phys. 44, 3834 (1966).
[20]L. Wolniewicz, J. Chem. Phys. 43, 1087 (1965).
[21]D. R. Bates, K. L. Bell, and A. E. Kingston, Proc. Phys. Soc. Lond. 91, 288 (1967).
[22]H. Hotop, E. Illenberger, H. Morgner, and A. Niehaus, Chem. Phys. Lett. 10, 493 (1971); H. Hotop, Radiat. Res. 59, 379 (1974).
[23]W. A. Miller, J. Chem. Phys. 52, 3563 (1970).
[24]A. P. Hickman and H. Morgner, J. Chem. Phys. 67, 5484 (1977).
[25]J. Fort, J. J. Laucagne, A. Pesnelle, and G. Watel, Chem. Phys. Lett. 37, 60 (1976).
[26]R. H. Neynaber and G. D. Magnuson, J. Chem. Phys. 62, 4953 (1975).